

Journal of Intelligent Material Systems and Structures

<http://jim.sagepub.com/>

A trapezoidal flexoelectric accelerometer

Wenbin Huang, Seol-Ryung Kwon, Shujun Zhang, Fuh-Gwo Yuan and Xiaoning Jiang
Journal of Intelligent Material Systems and Structures published online 7 June 2013
DOI: 10.1177/1045389X13491021

The online version of this article can be found at:

<http://jim.sagepub.com/content/early/2013/05/23/1045389X13491021>

Published by:



<http://www.sagepublications.com>

Additional services and information for *Journal of Intelligent Material Systems and Structures* can be found at:

Email Alerts: <http://jim.sagepub.com/cgi/alerts>

Subscriptions: <http://jim.sagepub.com/subscriptions>

Reprints: <http://www.sagepub.com/journalsReprints.nav>


Permissions: <http://www.sagepub.com/journalsPermissions.nav>

>> [OnlineFirst Version of Record](#) - Jun 7, 2013

[What is This?](#)

A trapezoidal flexoelectric accelerometer

Wenbin Huang¹, Seol-Ryung Kwon¹, Shujun Zhang², Fuh-Gwo Yuan¹ and Xiaoning Jiang¹

Journal of Intelligent Material Systems and Structures
0(0) 1–7
© The Author(s) 2013
Reprints and permissions:
sagepub.co.uk/journalsPermissions.nav
DOI: 10.1177/1045389X13491021
jim.sagepub.com


Abstract

In this article a new acceleration sensor using flexoelectric barium strontium titanate cantilever was designed, fabricated, and tested for vibration monitoring. The flexoelectric sensors were configured as a trapezoidal unimorph with a barium strontium titanate layer bonded onto a steel substrate. Seismic mass was attached to the unimorph tip to amplify the transverse flexoelectric response of the barium strontium titanate layer. The theoretical model was developed and validated by vibration tests using the prototyped flexoelectric unimorph. The prototyped accelerometer with thickness of 0.1 mm and length and width in millimeters showed a stable sensitivity of 0.84 pC/g over the frequency range of 100 Hz–1.6 kHz. The aging property of the flexoelectric material was demonstrated to be much better than that of the reported piezoelectric materials right after poling. Scaling effect analysis was also performed for flexoelectric unimorphs. The test results and initial scaling effect analysis indicate that micro/nano flexoelectric sensing holds promise for a broad range of applications.

Keywords

Flexoelectric, accelerometer, barium strontium titanate, flexoelectric unimorph

Introduction

High-performance low-cost miniaturized accelerometers are of great interest in automotives, consumer electronics, biomedical devices, industrial monitoring, and military applications. Among the various types of microaccelerometers, piezoelectric microaccelerometers offer attractive features such as high output impedance and simple structures. However, they face challenges such as poor low-frequency response, aging, depolarization and decreased performance at micro-/nanoscale (Yu and Lan, 2001). Recent studies on the flexoelectric effect suggest an alternative approach toward high-performance electromechanical sensors due to the greatly enhanced effective piezoelectricity of the miniaturized flexoelectric structures (Majdoub et al., 2008).

The flexoelectric effect describes the coupling between the mechanical strain gradient and electric polarization in a given material. The phenomenon is characterized by a tensorial relationship

$$P_l = \mu_{ijkl} \frac{\partial \varepsilon_{ij}}{\partial x_k} \quad (1)$$

where P_l is the component of flexoelectric polarization; μ_{ijkl} is the flexoelectric coefficients, a fourth rank tensor; ε_{ij} is the mechanical strain tensor; and x_k is the

direction of the gradient in ε_{ij} . For a cubic crystal, the nonzero components of μ_{ijkl} are μ_{1111} , μ_{1122} , and μ_{2233} or μ_{11} , μ_{12} , and μ_{44} in matrix notation.

Kogan (1964) discussed the electric polarization induced in a centric crystal by inhomogeneous deformation in 1964. Tagantsev (1986) combined dynamic bulk flexoelectricity, static flexoelectricity, surface flexoelectricity, and surface piezoelectricity in an exhaustive theoretical analysis. Through the theoretical study of a simple elemental cubic model for centrosymmetric materials, Resta (2010) suggested that the flexoelectric tensor is a bulk response of the solid, without surface contribution in the thermodynamic limit. However, surface effect in a more complex symmetry group still remains unclear. Unlike the piezoelectric effect that is limited to 20 crystal symmetry groups, all insulate solids exhibit flexoelectricity. Cross's group experimentally

¹Department of Mechanical and Aerospace Engineering, North Carolina State University, Raleigh, NC, USA

²Materials Research Institute, Pennsylvania State University, University Park, PA, USA

Corresponding author:

Xiaoning Jiang, Department of Mechanical and Aerospace Engineering, North Carolina State University, Raleigh, NC 27695, USA.
Email: xjiang5@ncsu.edu

measured the flexoelectric coefficients of certain ferroelectrics, including lead magnesium niobate (PMN), barium strontium titanate (BST), lead strontium titanate (PST), barium titanate (BT), and lead zirconate titanate (PZT). Among these ferroelectric materials, BST has a $\mu_{12} = 100 \mu\text{C}/\text{m}$ at its Curie temperature (about one order of magnitude higher than that of PMN and PZT) (Cross, 2006). Polymers such as polyvinylidene fluoride (PVDF) were studied recently (Baskaran et al., 2011; Chu and Salem, 2012). Zubko et al. (2007) reported experimental characterization of all the components of the flexoelectric tensor for SrTiO_3 (ST), while Maranganti and Sharma (2009) made atomistic predictions of flexoelectric properties for both BT and ST. It was predicted by Majdoub et al. (2008) that flexoelectricity can greatly enhance the piezoelectricity of a BT cantilever when the feature size shrinks to nanometer range. This was confirmed by the recent finding of the giant flexoelectric effect in ferroelectric epitaxial thin films, which can be utilized for polarization rotation (Catalan et al., 2011; Lee et al., 2011).

In order to characterize flexoelectric materials, specific structures have been studied to generate a large mechanical strain gradient. Truncated pyramids and flexural beams are the two main structures yielding longitudinal and transverse strain gradients, respectively. Fu et al. (2007) demonstrated a concept of fabricating piezoelectric composites with nonpiezoelectric components, that is, truncated pyramid structures. Chu et al. (2009) fabricated a flexural mode composite with BST beams whose effective piezoelectric coefficient could reach up to 4350 pC/N. Therefore, there is a need to conduct flexoelectric device study utilizing the promising flexoelectric materials and structures.

In this article, a flexural mode accelerometer based on the BST-steel unimorph with a seismic mass was, for the first time, designed, fabricated, and tested. Static theoretical analysis was conducted for flexoelectric vibration sensing. Frequency responses of the accelerometer were obtained using finite element analysis (FEA) and compared with experimental measurements.

In addition, flexoelectric aging experiments were performed, followed by a scaling effect analysis for flexoelectric microaccelerometers.

Sensor design and experimental setup

Flexoelectric accelerometer modeling

Similar to piezoelectric accelerometers (Kim et al., 2012; Yu and Lan, 2001), there can be broadly categorized into three basic operating modes of flexoelectric transductions: compression mode, shear mode, and flexural mode or bending mode. Figure 1 shows the corresponding structures of piezoelectric and flexoelectric accelerometers. In order to generate strain gradient instead of homogeneous strain in the structure of compression or shear mode, the shape of the flexoelectric component needs to be tapered. In contrast to its piezoelectric counterpart, the electrode of the shear mode flexoelectric accelerometer should be patterned on the side walls of the sensor. These specific requirements of compression and shear mode flexoelectric transducers present fabrication challenges. Bending mode transducers, however, have better sensitivity and easier manufacturability for microaccelerometer and can be fabricated using flexoelectric thin or thick films. For all these reasons, the bending mode design was adopted in our study. The following section will focus on the modeling of the bending type flexoelectric accelerometer.

The accelerometer studied in this article is configured to be a flexoelectric unimorph with seismic mass attached at the tip, as shown in Figure 2. The unimorph consists of a flexoelectric top layer and a suspension layer underneath. A rectangular-shaped cantilever usually has a large stress concentration in the base. Trapezoidal cantilever could generate more uniform strain and strain gradient distributions along the length direction by eliminating the stress concentration, thus to improve the sensing range of the accelerometer (Benasciutti et al., 2010). Trapezoidal cantilever also raises the resonance frequency of the sensor.

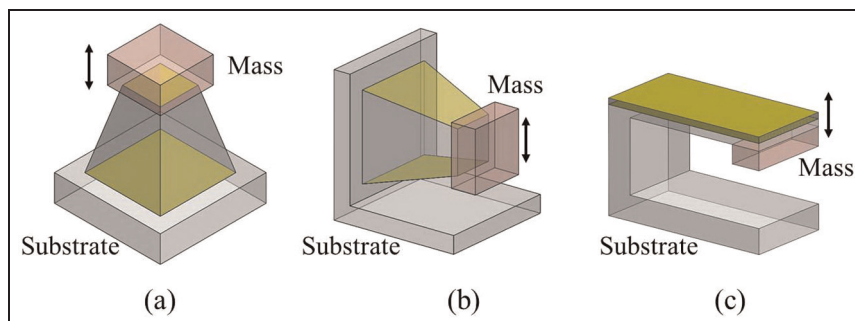


Figure 1. Basic structures of flexoelectric accelerometers (shaded layers represent the electrodes on the flexoelectric components): (a) compression, (b) shear, and (c) bending.

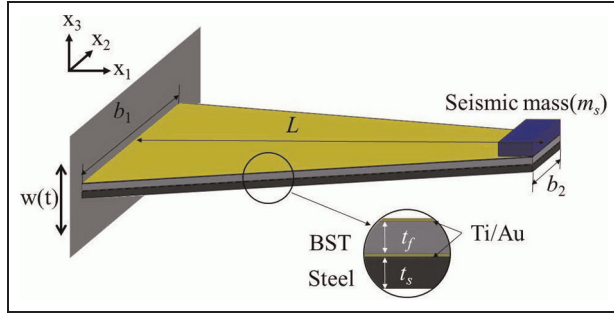


Figure 2. Schematic view of a flexoelectric unimorph accelerometer.

BST: barium strontium titanate.

In case that an acceleration is applied on the structure, the inertial force of seismic masses could bend the unimorph, which induces a nonuniform transverse strain along x_1 axis in the flexoelectric layer with a gradient along its thickness direction (x_3 axis). Based on Bernoulli–Euler beam theory, the curvature κ of a flexoelectric unimorph cantilever under bending moment can be given as (Smits and Choi, 1991)

$$\kappa(x_1) = \frac{12M(x_1)s_{11}^s s_{11}^f (s_{11}^s t_s + s_{11}^f t_f)}{Kb(x_1)} \quad (2)$$

where

$$K = 4s_{11}^f s_{11}^s t_s (t_f)^3 + 4s_{11}^s s_{11}^f t_f (t_s)^3 + (s_{11}^f)^2 (t_s)^4 + (s_{11}^s)^2 (t_f)^4 + 6s_{11}^f s_{11}^s (t_s)^2 (t_f)^2 \quad (3)$$

where the super- or subscript f denotes the upper flexoelectric element and s denotes the lower steel element, while s_{11} , t , and $b(x_1)$ are the elastic modulus, thickness, and width of the element, respectively. $b(x_1)$ can be written as

$$b(x_1) = \frac{b_1 - b_2}{L}(L - x_1) + b_2 \quad (4)$$

where b_1 and b_2 are the width at the tip and clamping end of the unimorph. L is the length of the unimorph.

$M(x_1)$ is the bending moment applied along the unimorph, which can be expressed as

$$M(x_1) = m_s a (L - x_1) \quad (5)$$

where m_s is the mass of the seismic mass and a is the acceleration. The strain gradient of the unimorph can be determined as

$$\frac{\partial \varepsilon_{11}}{\partial x_3} = \frac{\partial^2 w(x_1)}{\partial x_1^2} = \kappa(x_1) \quad (6)$$

where $w(x_1)$ is the vertical deflection of the unimorph along the x_1 direction. Thus, the total charge induced

can be obtained by integrating the polarization along the length as

$$Q = \int_0^L \mu_{12} \frac{\partial \varepsilon_{11}}{\partial x_3} b(x_1) dx_1 = \frac{6\mu_{12} s_{11}^s s_{11}^f (s_{11}^s t_s + s_{11}^f t_f) L}{K} m_s a \quad (7)$$

The sensitivity S_Q of the flexoelectric accelerometer is as follows

$$S_Q = \frac{Q}{a} = \frac{6\mu_{12} s_{11}^s s_{11}^f (s_{11}^s t_s + s_{11}^f t_f) L}{K} m_s \quad (8)$$

FEA

As there is no coupled-field electromechanical flexoelectric model in any existing finite element software, we chose the solid mechanics module of COMSOL Multiphysics to simulate the frequency response of the flexoelectric accelerometer. As a first step, a modal analysis was performed to calculate the natural frequency and harmonics of the accelerometer. The frequency domain analysis was implemented next to obtain the frequency response of the accelerometer. Excitation of sinusoidal form was applied at the clamping end of the cantilever assuming constant excitation acceleration amplitude. The other side was set as free. Strain gradient components in the flexoelectric layer can be estimated by subtracting the corresponding strain tensors in the top and the bottom surfaces and then dividing it by the layer thickness. Multiplying the flexoelectric coefficient with the strain gradient and integrating along the whole sensor area yield the expected sensor charge output.

BST ceramic preparation

Conventional solid state procedure was used to prepare $\text{Ba}_{0.65}\text{Sr}_{0.35}\text{TiO}_3$ ceramics using raw materials including BaCO_3 (99.9%, Alfa Aesar), SrCO_3 (99.9%, Alfa Aesar), and TiO_2 (99.99%, Alfa Aesar). The composition of BST was selected to be Ba:Sr = 65%:35%. All the materials were weighed according to the nominal composition. The powders were milled in anhydrous ethanol for 1 day and then calcined at 1200°C for 2 h to decompose the carbonate and synthesize BST powder. The obtained powder was remilled and double-calcined at the same temperature and then granulated through an 80-mesh sieve. The powder was pressed into pellets with >30 mm diameter using a cold isotropic pressing at 30 klpf/in². All the samples were sintered at temperatures in the range of 1300°C – 1380°C . After sintering, the samples were cooled down to room temperature at $3^\circ\text{C}/\text{min}$ in an oxygen atmosphere. The dielectric constant of BST at room temperature is about 8000, and the maximum dielectric constant is about 14,000 at the

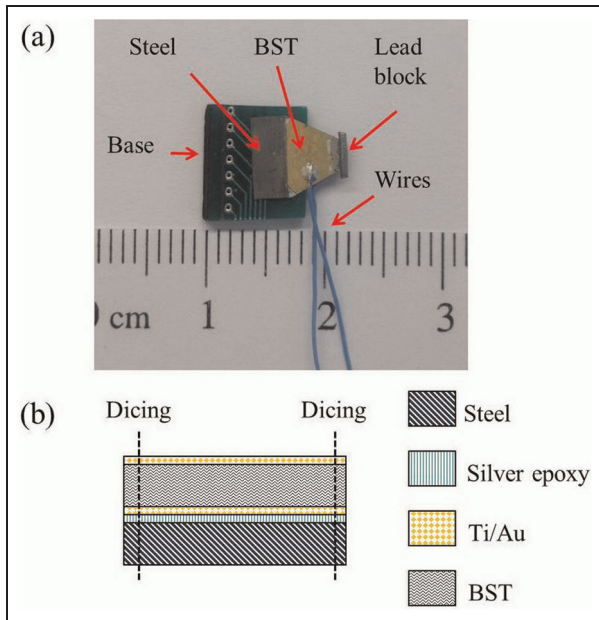


Figure 3. Photographic and schematic pictures of the accelerometer: (a) top view and (b) side view. BST: barium strontium titanate.

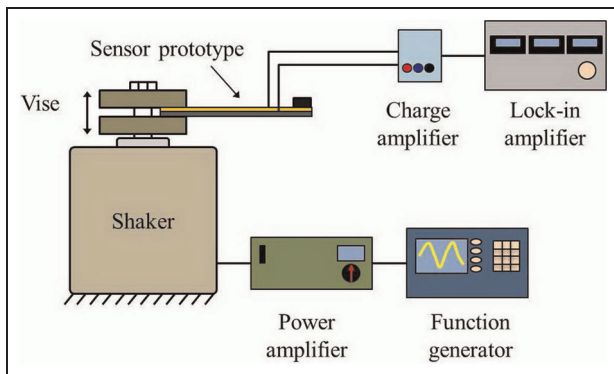


Figure 4. Experimental setup for the flexoelectric acceleration test.

Table 1. Dimensions of the trapezoidal accelerometer.

b_1	b_2	L	t_f	t_s	m_s
7 mm	2 mm	3 mm	50 μm	50 μm	15 mg

Curie temperature of 18°C. By using the cantilever beam-based direct measurement introduced in another article (Huang et al., 2011), the transverse flexoelectric coefficient μ_{12} was measured to be about 20 $\mu\text{C}/\text{m}$.

Sensor fabrication

The prototyped accelerometer is shown in Figure 3. First, the bottom side of a 700- μm BST plate was

sputtered with 50 \AA of Ti and 1000 \AA of gold as an electrode. The BST plates were then bonded onto the 50- μm steel plate with high-strength silver epoxy (EO-23M, Epoxyset). Normal pressure of about 1 MPa was applied to make the bonding layer uniform and thin, thus to ensure good adhesion and conductivity between BST and steel layers. BST layer was lapped down to 50 μm thick, and the top surface of BST layer was then electroded. This composite was diced into the trapezoid shape with the dimensions shown in Table 1 using a Disco 321 dicing saw. Finally, a lead block (3 mm \times 0.6 mm \times 0.6 mm) was attached onto the tip of the accelerometer as a seismic mass using superglue bonding. The accelerometer was bonded to a thick plastic base with superglue to make it convenient to be clamped in the vise.

Experimental setup

The experimental setup for sensor test is shown in Figure 4. The sensor was attached to a vibration exciter (Model ES020, KCF Technologies). A function generator (Model AFG3101, Tektronix) was used to generate a sinusoidal signal that was amplified by a power amplifier (Type 2706, Brüel & Kjær) and then applied to the vibration exciter to generate vibration with designed frequency and amplitude. The output charge signal from the sensor was converted and amplified to voltage signal through a charge amplifier (Type 2635, Brüel & Kjær), which was recorded through a lock-in amplifier (Model SR830, Stanford Research Systems). A commercial accelerometer (Model 352C22, PCB Piezotronics) was used as a reference to measure the acceleration from the vibration exciter. This acceleration was also recorded on the oscilloscope through a signal conditioner (Model 482A16, PCB Piezotronics). The generated charge from the flexoelectric accelerometer was recorded as a function of vibration frequency (10–4000 Hz) and base acceleration (0.2–3 \times g).

Results and discussion

Modeling results

Parameters used for the modeling are shown in Table 2. The sensor was meshed automatically with free tetrahedral elements in normal-level size. The total number of elements is 2785. The first-order resonance frequency of the accelerometer was found to be 3312 Hz. Excitation frequency was swept from 10 to 4000 Hz to obtain the frequency response of the sensor. The finite element modeling results are shown in Figure 5. In the low frequency range that is far away from the resonance frequency of the system, the FEA presents a flat frequency response with the sensitivity of 1.02 pC/g. To obtain the static analytical results, the

Table 2. Material properties used in the modeling.

Materials	BST	Steel
Young's modulus (GPa)	153	210
Poisson's ratio	0.33	0.3

BST: barium strontium titanate.

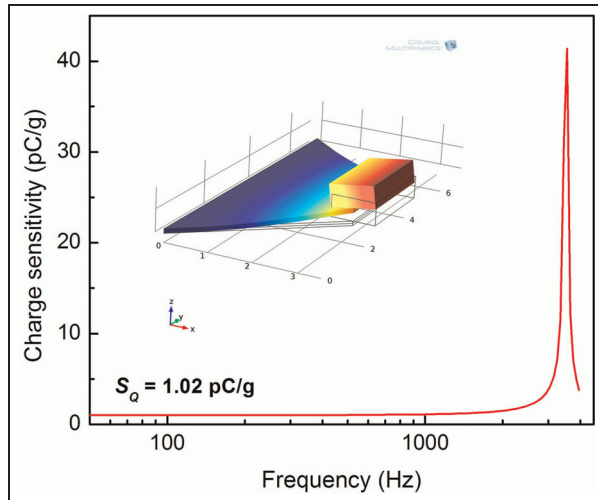


Figure 5. Finite element analysis of the sensor using COMSOL code indicating the frequency range and the charge sensitivity.

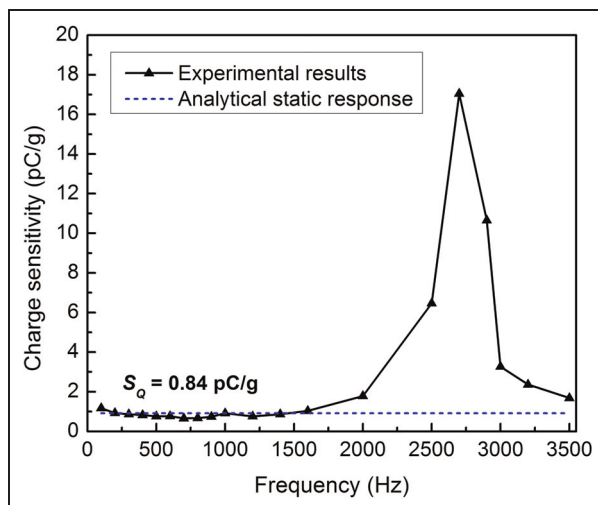


Figure 6. Comparison of measured frequency response with the analytical solution.

parameters in Tables 1 and 2 were substituted into equation (8). Charge sensitivity of the accelerometer at flat frequency response was calculated to be 0.89 pC/g. As can be seen from equation (8), the sensitivity of the accelerometer is determined by the seismic mass and the flexoelectric constant. Proper sensitivity can be applied to a specific application.

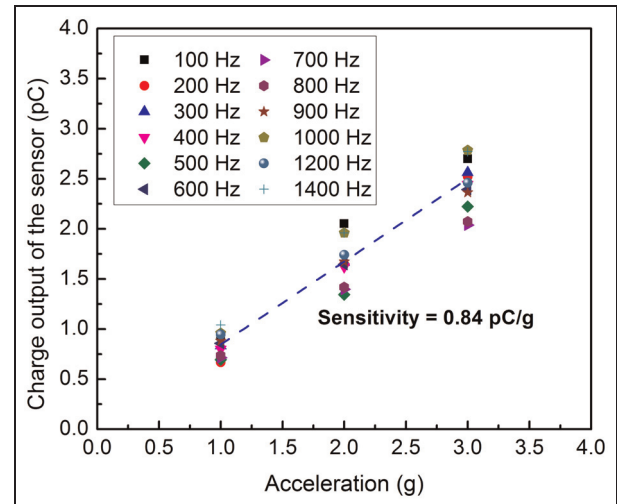


Figure 7. Sensor charge output under different frequencies and acceleration ranges.

Experimental results

As shown in Figure 6, the experimental results reveal a stable sensitivity of 0.84 pC/g in the low frequency range. The working frequency with the flat frequency response reaches 1600 Hz. The resonance frequency of the sensor system is 2800 Hz. It is essential to stress that equation (6) is only applicable to the cantilever with infinitesimal deflection, otherwise large error would exist (Baskaran et al., 2012; Bisplinghoff et al., 2002). The maximum deflection in the test is about 6.5 μm with the angle of 0.2°. Such small deformation could ensure the precision of theoretical estimation. Figure 7 shows the sensor output as a function of acceleration under different frequencies. The lower charge sensitivity compared with the FEA and analytical results may be rooted in the absence of rigid and precise clamping of the accelerometer. Nonideal bonding between the BST layer and the suspension layer could inhibit the full strain transmission, thus diminishing the sensor sensitivity. Imprecise clamping could also decrease the natural frequency by increasing the effective sensor length. The additional mass of bonded electric wires could reduce the resonance frequency as well.

Aging rate tests

It has been known that piezoelectric ceramics have a long-term aging problem after polarization (Koh et al., 2004). Hence, when these materials are used in sensors and actuators, the decrease of efficiency or sensitivity should be considered and compensated properly to maintain the accuracy of devices. Aging of piezoelectric ceramics occurs rapidly in the first few hours after removal of the poling field. After few days, the changes of piezoelectric constants become much more slowly.

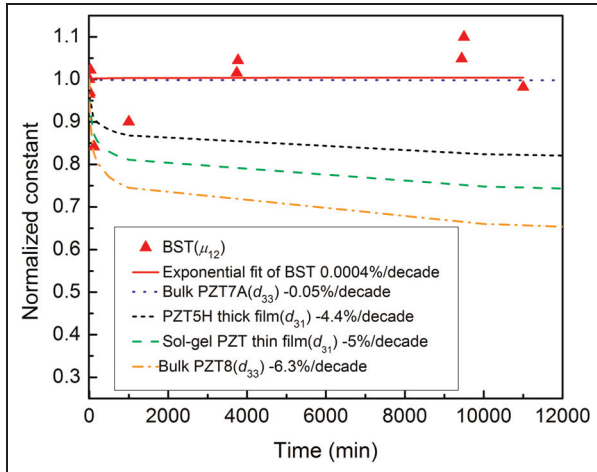


Figure 8. Aging of the piezoelectric (right after poling) and flexoelectric coefficients.

BST: barium strontium titanate; PZT: lead zirconate titanate.



Figure 9. Schematic picture of a flexoelectric microaccelerometer.

Generally, the aging rate A can be defined by the equation, $y(t)/y(t_0) = 1 + A \times \log(t/t_0)$, where y is the concerned materials property, t_0 is an arbitrary time when the measurement started, and t is the elapsed time (Mason, 1955).

Unlike piezoelectric ceramics, flexoelectric materials do not have the aging problem due to the absence of remnant polarization during utilization of the flexoelectric materials. To demonstrate the zero aging-free behavior of flexoelectric materials, the μ_{12} coefficient was measured with respect to time and compared with the reported aging properties of the piezoelectric coefficients in piezoelectric materials (Glynne-Jones et al., 2001; Shepard et al., 1999). The piezoelectric coefficients (d_{33} and d_{31}) and flexoelectric coefficient (μ_{12}) were normalized by deriving the real-time values to that measured just after poling. As shown in Figure 8, the fit of BST has 0.0004% per decade aging rate, which is in the error range and can be considered as 0. Compared to other piezoelectric materials, flexoelectric properties are invariant over time. Scattered data of BST may be due to the inconsistent clamping and environmental variation of the test area.

Scaling analysis

Smaller accelerometers consume less chip size and lead to reduced manufacturing costs (Tadigadapa and Mateti, 2009). In addition, miniaturized sensors enable new sensor applications, for example, in mobile devices or chip cards. Therefore, the sensor shrink is especially important for consumer products that require small, low-cost and low-power sensors.

For a thin-film flexoelectric microaccelerometer, as shown in Figure 9, the thickness of a flexoelectric thin-film layer can be submicron, and the thickness of the suspension layer (e.g. silicon layer) is usually in the range of tens of microns. Since the sensing layer is much thinner and shorter than the substrate, it can be assumed that the longitudinal stress in the flexoelectric layer is constant and equals to the maximum stress value at the base. The polarization induced in the flexoelectric layer is given by

$$P = \mu_{12} \frac{\partial \varepsilon_{11}}{\partial x_3} = \frac{2\mu_{12}\varepsilon_{max}}{t_s} \quad (9)$$

The sensitivity of the microaccelerometer can be obtained

$$S_f \propto \frac{P}{\varepsilon_{max}} = \frac{2\mu_{12}}{t_s} \quad (10)$$

For a piezoelectric microaccelerometer with the same configuration, the effective sensitivity can be presented as

$$P = e_{31}\varepsilon_{max} \quad (11)$$

where e_{31} is the transverse piezoelectric strain coefficient and its sensitivity is given as

$$S_p \propto e_{31} \quad (12)$$

From the comparison between equations (9) and (11), it can be observed that high acceleration sensitivity can be obtained from the flexoelectric microaccelerometer because of the scaling effect, which is nonexistent in its piezoelectric counterpart. For example, assuming that the piezoelectric transverse coefficient e_{31} of sol-gel PZT is about 8.3 C/m^2 (Dubois and Murali, 1999), and μ_{12} of BST is about $20 \text{ } \mu\text{C/m}$ as we measured, the effective sensitivity of the flexoelectric sensor will exceed that of the same-sized piezoelectric microaccelerometer when the thickness of the silicon substrate is less than $4.8 \text{ } \mu\text{m}$, and the thicknesses of piezo film and flexoelectric film are less than $1 \text{ } \mu\text{m}$. Actually, flexoelectric sensing can exhibit greater superiority by considering that μ_{12} can be as high as $100 \text{ } \mu\text{C/m}$ (Ma and Cross, 2002), suggesting that flexoelectric micro-/nanoaccelerometers are promising for advanced vibration sensing applications.

Conclusion

A trapezoidal flexoelectric unimorph accelerometer using $\text{Ba}_{0.65}\text{Sr}_{0.35}\text{TiO}_3$ was designed, prototyped, and tested. The static analytic analysis and frequency response based on FEA were conducted. The accelerometer provides a sensitivity of 0.84 pC/g in the working frequency of up to 1.6 kHz. In addition, flexoelectric materials exhibit aging-free characteristics. The sensitivity of the flexoelectric microaccelerometer can be potentially enhanced through size reduction due to the scaling effect of flexoelectric unimorph structures.

Funding

This material is based on work supported by, or in part by, the US Army Research Laboratory and the US Army Research Office under contract/grant number W911NF-11-1-0516 and in part by National Science Foundation under grant number CMMI-1068345.

References

- Baskaran S, He X, Chen Q, et al. (2011) Experimental studies on the direct flexoelectric effect in alpha-phase polyvinylidene fluoride films. *Applied Physics Letters* 98(24): 242901–242903.
- Baskaran S, He X, Wang Y, et al. (2012) Strain gradient induced electric polarization in α -phase polyvinylidene fluoride films under bending conditions. *Journal of Applied Physics* 111: 014109.
- Benasciutti D, Moro L, Zelenika S, et al. (2010) Vibration energy scavenging via piezoelectric bimorphs of optimized shapes. *Microsystem Technologies* 16(5): 657–668.
- Bisplinghoff RL, Mar JW and Pian TH (2002) *Statics of Deformable Solids*, vol. 7. Dover Publications, Mineola, N.Y. pp. 194–198.
- Catalan G, Lubk A, Vlooswijk A, et al. (2011) Flexoelectric rotation of polarization in ferroelectric thin films. *Nature Materials* 10(12): 963–967.
- Chu B and Salem DR (2012) Flexoelectricity in several thermoplastic and thermosetting polymers. *Applied Physics Letters* 101(10): 103905.
- Chu BJ, Zhu WY, Li N, et al. (2009) Flexure mode flexoelectric piezoelectric composites. *Journal of Applied Physics* 106(10): 104109.
- Cross LE (2006) Flexoelectric effects: charge separation in insulating solids subjected to elastic strain gradients. *Journal of Materials Science* 41(1): 53–63.
- Dubois MA and Muralt P (1999) Measurement of the effective transverse piezoelectric coefficient $e_{31,f}$ of AlN and $\text{Pb}(\text{Zr}_x\text{Ti}_{1-x})\text{O}_3$ thin films. *Sensors and Actuators A: Physical* 77(2): 106–112.
- Fu JY, WY Zhu, N Li, et al. (2007) Gradient scaling phenomenon in microsize flexoelectric piezoelectric composites. *Applied Physics Letters* 91(18): 182910.
- Glynne-Jones P, Beeby SP and White NM (2001) A method to determine the ageing rate of thick-film PZT layers. *Measurement Science & Technology* 12(6): 663–670.
- Huang WB, Kim K, Zhang SJ, et al. (2011) Scaling effect of flexoelectric $(\text{Ba,Sr})\text{TiO}_3$ microcantilevers. *Physica Status Solidi-Rapid Research Letters* 5(9): 350–352.
- Kim K, Zhang S, Salazar G, et al. (2012) Design, fabrication and characterization of high temperature piezoelectric vibration sensor using YCOB crystals. *Sensors and Actuators A: Physical* 178(0): 40–48.
- Kogan SM (1964) Piezoelectric effect during inhomogeneous deformation and acoustic scattering of carriers in crystals. *Soviet Physics-Solid State* 5(10): 2069–2070.
- Koh JH, Jeong SJ, Ha MS, et al. (2004) Aging of piezoelectric properties in $\text{Pb}(\text{MgNb})\text{O}_3\text{-Pb}(\text{ZrTi})\text{O}_3$ multilayer ceramic actuators. *Journal of Applied Physics* 96(1): 544–548.
- Lee D, Yoon A, Jang SY, et al. (2011) Giant flexoelectric effect in ferroelectric epitaxial thin films. *Physical Review Letters* 107(5): 057602.
- Ma WH and Cross LE (2002) Flexoelectric polarization of barium strontium titanate in the paraelectric state. *Applied Physics Letters* 81(18): 3440–3442.
- Majdoub MS, Sharma P and Cagin T (2008) Enhanced size-dependent piezoelectricity and elasticity in nanostructures due to the flexoelectric effect. *Physical Review B* 77(12): 125424.
- Maranganti R and Sharma P (2009) Atomistic determination of flexoelectric properties of crystalline dielectrics. *Physical Review B* 80(5): 054109.
- Mason WP (1955) Aging of the properties of barium titanate and related ferroelectric ceramics. *Journal of the Acoustical Society of America* 27(1): 73–85.
- Resta R (2010) Towards a bulk theory of flexoelectricity. *Physical Review Letters* 105(12): 127601.
- Shepard JF, Chu F, Kanno I, et al. (1999) Characterization and aging response of the d_{31} piezoelectric coefficient of lead zirconate titanate thin films. *Journal of Applied Physics* 85(9): 6711–6716.
- Smits JG and Choi WS (1991) The constituent equations of piezoelectric heterogeneous bimorphs. *IEEE Transactions on Ultrasonics Ferroelectrics and Frequency Control* 38(3): 256–270.
- Tadigadapa S and Mateti K (2009) Piezoelectric MEMS sensors: state-of-the-art and perspectives. *Measurement Science & Technology* 20(9): 092001.
- Tagantsev AK (1986) Piezoelectricity and flexoelectricity in crystalline dielectrics. *Physical Review B* 34(8): 5883–5889.
- Yu JC and Lan CB (2001) System modeling of microaccelerometer using piezoelectric thin films. *Sensors and Actuators A: Physical* 88(2): 178–186.
- Zubko P, Catalan G, Buckley A, et al. (2007) Strain-gradient-induced polarization in SrTiO_3 single crystals. *Physical Review Letters* 99(16): 167601.